Structural Studies on the Ca^{2+}-binding Domain of Human Nucleobindin (Calnuc)

Eva de Alba and Nico Tjandra*

Laboratory of Biophysical Chemistry, National Heart, Lung, and Blood Institute, National Institutes of Health, 50 Center Drive, Bethesda, Maryland 20892

Received April 7, 2004; Revised Manuscript Received June 11, 2004

ABSTRACT: Nucleobindin, also known as calnuc, participates in Ca^{2+} storage in the Golgi, as well as in other biological processes that involve DNA-binding and protein−protein interactions. We have determined the three-dimensional solution structure of the Ca^{2+}-binding domain of nucleobindin by NMR showing that it consists of two EF-hand motifs. The NMR structure indicates that the ϕ and ψ angles of residues in both motifs are very similar, despite the noncanonical sequence of the C-terminal EF-hand, which contains an arginine residue instead of the typical glycine at the sixth position of the 12-residue loop. The relative orientation of the α-helices in the N-terminal EF-hand falls within the common arrangement found in most EF-hand structures. In contrast, the noncanonical EF-hand deviates from the average orientation. The two helix-loop-helix moieties are in the open conformation characteristic of the Ca^{2+}-bound state. We find that both motifs bind Ca^{2+} with apparent dissociation constants of 47 and 40 μM for the noncanonical and the canonical EF-hand, respectively. The Ca^{2+}-binding domain of nucleobindin is unstructured in the absence of Ca^{2+} and folds upon Ca^{2+} addition. NMR relaxation data and structural studies of the folded domain indicate that it undergoes slow dynamics, suggesting that it is floppier and less compact than a globular domain.

A large number of biological processes depend on calcium signaling, on the regulation of calcium concentration in the different cell organelles, or on both. One of the most common protein structural motifs involved in Ca^{2+}-binding is the helix-loop-helix motif of the EF-hand protein super family. EF-hand proteins can be divided into two major classes: (1) the Ca^{2+} sensors, such as calmodulin and troponin C, which translate Ca^{2+} signals through their interaction with target proteins and (2) the Ca^{2+} buffers, such as calbindin D_{9k} and parvalbumin, which are involved in Ca^{2+} homeostasis (*1*).

Nucleobindin (calnuc) (*2*), a protein predicted to contain two EF-hand moieties, is highly abundant in the Golgi apparatus where it is known to be involved in Ca^{2+} storage (*3*, *4*). Nucleobindin has been found attached to the luminal surface of the Golgi membranes and in the cytoplasm where it interacts with $G_{\alpha i3}$ through its Ca^{2+}-binding domain (*5*, *6*). Nucleobindin is also secreted into the culture media, although no function has been suggested for this extracellular pool (*7*). $G_{\alpha i2}$ has also been shown to interact with nucleobindin, and it has been proposed that this interaction may take place in the nucleus (*8*).

Nucleobindin is a multifunctional protein, since it binds DNA, contains a signal peptide and a leucine zipper motif. The later possibly participates in dimerization or interactions with other proteins (*9*). Nucleobindin is expressed in a large variety of tissues. Its amino acid sequence is well conserved from flies to humans, suggesting that it carries out important biological functions (*10*). Figure 1A shows a schematic representation of the primary structure of nucleobindin indicating the location of the different predicted motifs.

Nucleobindin was originally discovered as a factor promoting the formation of antibodies against single- and double-stranded DNA, both in vivo and in vitro in a cell line established from MRL/l lupus-prone mouse (*11*, *12*). The putative DNA-binding domain of nucleobindin (i.e., the basic-rich region, Figure 1A) is separated from the leucine zipper by the Ca^{2+}-binding domain. Because this arrangement is different from that found in regular transcription factors, where a helix-loop-helix moiety connects the basic region and the leucine zipper, it is unlikely that DNA-binding occurs through the classical mechanism.

Nucleobindin has been shown to interact with cyclooxygenases 1 and 2. These proteins reside in the endoplasmatic reticulum and the nuclear envelope and catalyze the conversion of arachidonate to prostanoids. Accordingly, nucleobindin has been portrayed as a potential regulator of these enzymes (*13*).

Another binding partner of nucleobindin is necdin, a growth suppressor expressed in neurons, which interacts with viral oncoproteins and cellular transcription factors. The interaction seems to involve the Ca^{2+}-binding domain of nucleobindin (*14*).

All of these observations suggest that nucleobindin carries out multiple functions through its Ca^{2+}-binding, DNA-binding, and leucine zipper domains and through its ability to interact with proteins involved in different biological processes. According to the reported data, nucleobindin may have a dual function as a calcium sensor and a calcium buffer. To understand the role played by the Ca^{2+}-binding domain of nucleobindin in these processes, it is necessary

* To whom correspondence should be addressed. E-mail: nico@helix.nih.gov. Phone: 301-402-3029. Fax: 301-402-3404.

10.1021/bi049310a
Published on Web 07/17/2004

A

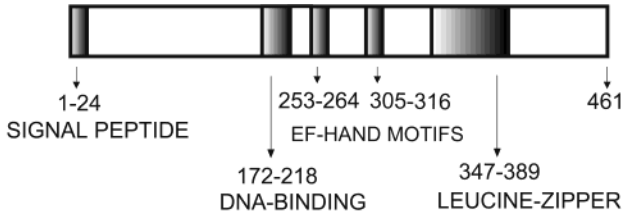

B

```
nucleobindin   DINSDGVLDEQE(253-264)DTNQDRLVTLEE (305-316)

CALCIUM SENSORS

calmodulin     DKDGDGTITTKE (20-31) DADGNGTIDFPE (65-76)  DKDGNGYISAAE (93-104) DIDGDGQVNYEE (129-140)

troponin C     DEDGSGTVDFDE (65-76) DKNADGYIDLEE (105-116)DKNNDGRIDYDE (141-152)

calcineurin B DLDNSGSLSVEE (30-41) DTDGNGEVDFKE (62-73)  DMDKDGYISNGE (99-110) DKDGDGRISFEE (140-151)

neurocalcin    RDCPSGHLSMEE (35-46)*DANGDGTIDFRE (72-83)  DLDGNGYISKAE (108-119)DTNRDGKLSLEE (156-167)

caltractin     DADGTGTIDVKE (41-52) DKEGTGKMNFGD (77-88)* DDDETGKISFKN(114-125)*DRDGDGEVSEQE(150-161)

S100           SGREGDKHKLKKSE (18-31) DNDGDGECDFQE (61-72)

CALCIUM BUFFERS

parvalbumin    DKDKSGFIEEDE (51-62) DKDGDGKIGVDE (90-101)

calbindin D9k AAKEGDPDQLSKDE (17-30) DKNGDGEVSFEE (57-68)

calbindin D28k** DADGSGYLEGKE (23-34) GQRDDGKIGIVE (65-76)* DTDHSGFIETEE (110-121)

                 DSNNDGKLELTE(154-165)DQDGNGYIDENE (198-209)ALSDGGKLYRTD (239-250)*

*    potential ancestral calcium site
**   also functions as calcium sensor
```

FIGURE 1: (A) Location of the different predicted domains in the primary structure of human nucleobindin; (B) sequence alignment of the EF-hand motifs of nucleobindin and several proteins known to act as Ca^{2+} buffers and Ca^{2+} sensors. Start and end residues are shown in parentheses.

to investigate the structural characteristics of the domain and its Ca^{2+}-binding capabilities. We have solved the three-dimensional structure of the Ca^{2+}-binding domain of nucleobindin by NMR,[1] showing that it consists of two EF-hand motifs.

The comparison between the structure of nucleobindin and other EF-hand structures sheds light into the dual function of nucleobindin as Ca^{2+} storage (buffer) and Ca^{2+} sensor. The C-terminal EF-hand of nucleobindin contains an arginine in position 6 of the 12-residue loop instead of the common glycine (Figure 1B) (*15*). We demonstrate that both EF-hands bind Ca^{2+}, even though one of them has a noncanonical amino acid sequence. We measured the Ca^{2+} dissociation constants, which are similar for both EF-hand moieties. NMR data suggest that the domain lacks a well-defined tertiary structure in the absence of Ca^{2+}. Structural and relaxation studies indicate that nucleobindin's Ca^{2+}-binding domain is mobile due to conformational exchange and less compact than a globular domain.

[1] Abbreviations: NMR, nuclear magnetic resonance; HSQC, heteronuclear single quantum spectroscopy; NOE, nuclear Overhauser effect; NOESY, NOE spectroscopy; TOCSY, total correlation spectroscopy; TPPI, time proportional phase incrementation; RMSD, root mean square deviation; ppm, parts per million; HPLC, high-pressure liquid chromatography; EDTA, ethylenediaminetetraacetate.

MATERIALS AND METHODS

Protein Preparation. The ^{15}N and ^{13}C isotopically enriched calcium-binding domain of nucleobindin was expressed as a His-tagged protein in *Escherichia coli* strain BL21(DE3) codon plus RP using pET-15b vector (Novagen) in minimal medium with ^{13}C-glucose and $^{15}NH_4Cl$ as sole carbon and nitrogen sources. The induction of protein expression was performed at 37 °C by the addition of 1 mM isopropyl β-D-thiogalactopyranoside for 4 h. Cells were harvested and resuspended in 100 mL of buffer containing 5 mM imidazole, 500 mM NaCl, 20 mM Tris, pH 8.0, lysozyme, and serine protease inhibitor, 4-(2-aminoethyl)-benzenesulfonyl fluoride hydrochlorine. Cells were lysed by ultrasonication and cleared by centrifugation. The largest fraction of nucleobindin is soluble; however, a small portion was found in the cell pellet. To recover this portion, the pellet was treated with 5 M guanidinium hydrochloride. The supernatants from both batches were poured into different columns containing His-Bind resin (Novagen). Imidazol and guanidinium hydrochloride were eliminated by stepwise dialysis into solutions containing 5 mM $CaCl_2$ and decreasing amounts of imidazol and guanidinium hydrochloride. Biotinylated thrombin (Novagen) was used to cleave the histidine tag. ^{15}N-HSQC spectra of nucleobindin obtained from the soluble fraction

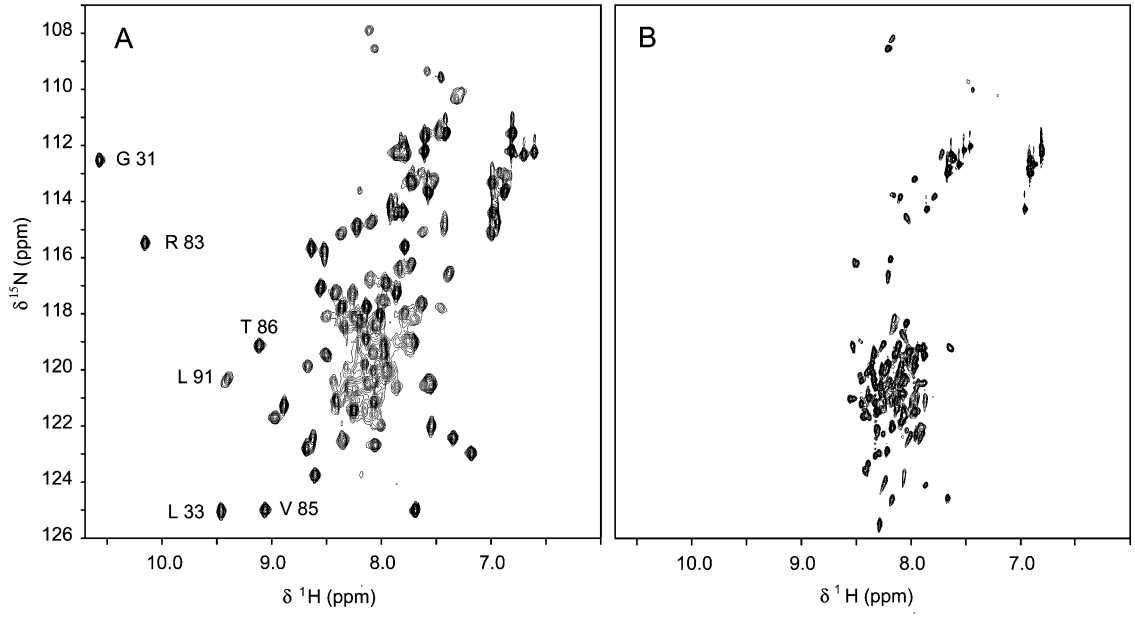

FIGURE 2: ^{15}N-HSQC of the Ca^{2+}-binding domain of human nucleobindin at 1 mM, pH 6.8, 300 K, and (A) 5 mM $CaCl_2$ or (B) 0 mM $CaCl_2$. Some of the residues that belong to the EF-hand loops with low-field-shifted ^{1}H chemical shifts are labeled.

and from the pellet were identical and characteristic of a folded protein. This is indicative that the protein can be refolded by removing guanidinium hydrochloride and the unfolding and refolding steps do not alter the protein conformation. To improve protein purity, the Ca^{2+}-binding domain of nucleobindin was further purified by reverse-phase HPLC before His-tag cleavage, then lyophilized and treated with biotinylated thrombin (Novagen) to cleave the histidine tag. Biotinylated thrombin was removed by adding streptavidin agarose (Novagen). Another step of reverse-phase HPLC purification was performed after thrombin cleavage. The eluted protein was lyophilized and washed with HPLC grade water to eliminate residual salt. The comparison between the ^{15}N-HSQC spectrum of the protein purified twice by HPLC and the ^{15}N-HSQC spectra of nucleobindin before HPLC purification indicates that unfolding by reverse-phase HPLC and subsequent refolding do not alter the protein conformation. Protein purity was checked by mass spectrometry.

The amino acid sequence of nucleobindin's calcium-binding domain is as follows: (GSHM)L_1KEVWEELD-G_{10}LDPNRFNPKT$_{20}$FFILHDINSD$_{30}$GVLDEQELE-A_{40}LFTKELEKVY$_{50}$DPKNEEDDMR$_{60}$EMEEERLRM-R_{70}EHVMKNVDTN$_{80}$QDRLVTLEEF$_{90}$LASTQRKEF$_{99}$. Residues GSHM do not belong to the sequence of native nucleobindin but remain after thrombin cleavage of the His-tag. In the full-length protein, L_1 corresponds to L_{228} and F_{99} to F_{326}.

NMR Data Collection for Structure Determination. NMR samples were prepared at ~1 mM protein concentration determined by light absorbance at 280 nm using an extinction coefficient of 6970 M^{-1} cm^{-1}. All samples contained 5 mM $CaCl_2$ and 0.1 mM NaN_3. The pH was adjusted to 6.8 by adding small amounts of 0.1 M KOH, and D_2O was added to 10% (v/v). Protein samples in Pf1 phage (ASLA) were prepared by mixing diluted solutions of phage and protein followed by concentration to ~0.8 mM protein and ~15 mg/mL phage.

NMR experiments were performed at 300 K on Bruker Avance 600 MHz and DRX 800 MHz spectrometers with triple resonance probes and triaxial gradients. The combined information obtained from the experiments, ^{15}N-HSQC, ^{13}C-HSQC, sensitivity-enhanced HNCO, CBCACONH, HNCACB, HBHACONH, HCCH-TOCSY (19.5 ms mixing time), CCONH, and HCCONH, was used to assign backbone ^{15}N and ^{1}H amide chemical shifts, as well as ^{1}H and ^{13}C chemical shifts of amino acid side chains. Four-dimensional ^{15}N- and ^{13}C-edited NOESY (114 ms mixing time), ^{13}C-^{13}C-edited NOESY (100 ms mixing time), and three-dimensional ^{15}N-edited NOESY (102 ms mixing time) were used for NOE assignment. For a review on the different three- and four-dimensional ^{13}C- and ^{15}N-edited NMR experiments for protein structure determination, see Bax and Grzesiek (*16*). NMR experiments for measuring residual dipolar couplings were performed on the phage-containing sample. There is a certain amount of overlapping in the center region of the ^{15}N-HSQC spectrum of the Ca^{2+}-binding domain of nucleobindin (vide infra, Figure 2). Therefore, dipolar couplings of amide NH bond vectors were measured using the three-dimensional HNCO experiment modified to allow ^{1}H−^{15}N coupling during ^{15}N evolution. For the identical reason, $C_\alpha H_\alpha$ dipolar couplings were measured using the three-dimensional experiment (HA)CA(CO)NH, in which ^{1}H−^{13}C coupling is active in the ^{13}C indirect dimension. The HNCO experiment was used to measure dipolar couplings of $C_\alpha C'$ bond vectors. In this case, C_α−C' coupling was active during carbonyl evolution. Dipolar couplings of CH_3 and CH moieties that belong to amino acid side chains were obtained with a ^{13}C-HSQC in which the peak intensity is modulated with ^{1}H−^{13}C coupling (*17*). All NMR experiments were processed with NMRPipe (*18*) and analyzed with PIPP (*19*).

Backbone ^{15}N Relaxation Measurements. Relaxation experiments were performed with 0.9 mM and 0.02 mM ^{15}N-labeled protein samples, pH 6.8, at 300 K on Bruker Avance 600 MHz, DRX 800 MHz, and DRX 600 MHz with cryoprobe for the 0.02 mM sample. All data sets consisted

of 128 × 512 complex data points that were zero-filled to 512 × 2048 data points. The ^{1}H carrier was positioned at the water frequency and the ^{15}N carrier at 116.5 ppm. States-TPPI quadrature detection in t_1 was used in all experiments (*20*).

The ^{15}N T_1 and $T_{1\rho}$ pulse sequences used (*21*) were modified to include the WATERGATE module (*22*), pulse field gradients (*23*), and a semiconstant time evolution period in t_1 (*24*). The $T_{1\rho}$ experiments utilized a continuous ^{15}N spin-lock (*25*) with a 2.5 kHz radio frequency field. $T_{1\rho}$ data were collected in an interleaved manner to minimize the effects of systematic errors. For $T_{1\rho}$ experiments, 32, 40, and 512 scans were used at 600, 800, and 600 MHz, respectively, with cryoprobe for the 0.02 mM sample. For T_1 experiments, 32 scans were used at 600 and 800 MHz. Relaxation times were calculated by fitting the dependence of the experimentally measured intensities with relaxation times to an exponentially decaying function. The relaxation times used in the $T_{1\rho}$ experiments were 10.0, 18.2, 33.6, 52.8, 57.6, 77.3, 88.8, and 98.4 ms (600 and 800 MHz) and 18.2, 33.6, 57.6, and 98.4 ms (600 MHz with cryoprobe) and for T_1 experiments 12, 44, 124, 244, 484, 804, 1044, and 1284 ms.

^{15}N-^{1}H heteronuclear NOE values were measured with a reported pulse program (*26*) and calculated from the ratio of peak intensities of experiments performed with and without ^{1}H presaturation;64 (600 MHz) and 80 (800 MHz) scans per t_1 point were used. The total duration of ^{1}H presaturation was 3.76 s. NOE values were corrected as previously described (*26*) to compensate for errors caused by incomplete ^{1}H magnetization recovery.

Structure Calculation. Peak intensities from NOESY experiments were translated into a continuous distribution of interproton distances. A summation averaging $[(\sum r^{-6})^{-1/6}]$ was used to obtain distances from intensities. For the majority of the distances, an error of ±30% of the distance was applied to obtain lower and upper limits. This error was increased for some distances that could be affected by spin diffusion processes. The program X-PLOR-NIH (*27*, *28*) was used for structure calculation. The fitting between the observed and calculated dipolar couplings was done using an alignment coordinate system. Initial values of the axial (D_a) and rhombic (R) components of the alignment tensor were calculated from the histogram distribution of dipolar couplings (*29*). Final values of D_a and R were obtained through a grid search by energy minimization. These are $D_a = -7.35$ Hz and $R = 0.57$. Residual dipolar couplings of NH, $C_\alpha H_\alpha$, $C_\alpha C'$, CH_3, and $C_\beta H_\beta$ (isoleucine, valine, and threonine residues) bonds were used as restraints. A quadratic harmonic potential was applied for all dipolar couplings except those belonging to residues of which the ^{15}N relaxation data indicate higher mobility than what is expected for secondary structure. In this case and for bond vectors that belong to amino acid side chains, a half-open square well penalty function was used (*17*).

Hydrogen bonds were defined according to the experimentally determined secondary structure of the protein. Two restraints were used per hydrogen bond (e.g., $r_{NH-O} = 1.5-2.5$ Å and $r_{N-O} = 2.4-3.6$ Å). The TALOS program was used to obtain ϕ and ψ restraints only for those residues with statistically significant predictions (*30*). No structural restraints were used to calculate or model the position of the calcium ions.

Ca^{2+} Titration Experiments. The Ca^{2+}-binding domain of human nucleobindin was treated with 5 mM EDTA and vortexed for 30 min to remove Ca^{2+}. Sephadex G-25 M resin first equilibrated with 5 mM EDTA and second with Chelex resin-treated HPLC grade water was used to remove residual EDTA from the protein sample. The eluted protein was concentrated and Chelex resin-treated D_2O was added at 10% (v/v). The pH was adjusted to 6.8 with Chelex resin-treated KOH solution. The final protein concentration was 0.24 mM by light absorbance at 280 nm. The absence of EDTA was checked in the one-dimensional ^{1}H NMR spectrum of the sample.

It is important to mention that Chelex resin does not seem to have enough Ca^{2+}-binding affinity to remove Ca^{2+} from the protein, as we could test by NMR. EDTA instead removes Ca^{2+} efficiently.

One-dimensional ^{1}H projections of ^{15}N-HSQC spectra (2048 scans) were recorded at each point of the titration. Aliquots from a $CaCl_2$ stock solution were added such that the final Ca^{2+} concentrations were 0, 0.06, 0.08, 0.10, 0.12, 0.13, 0.15, 0.17, 0.20, 0.24, 0.28, 0.34, 0.38, and 0.46 mM. Each one-dimensional spectrum was baseline-corrected and calibrated with respect to the total amount of signal using as reference the spectrum of the 0 mM Ca^{2+} sample. The intensities of selected low-field shifted signals were followed throughout the titration.

Analysis of Ca^{2+} Titration Curves. The ratio between the intensities of a signal that belongs to the folded species and the same signal at the end of the titration was used to measure the ratio [Ca-bound protein]/[total protein]. The total concentration of added Ca^{2+} is known. The plot of these two quantities was fitted to the equation $y = [A_0 + A_1(10^{A_3(x-A_2)})]/[1 + 10^{A_3(x-A_2)}]$. The K_d values were obtained from the abscissa value at $y = 0.5$.

RESULTS AND DISCUSSION

Structural Studies on the Ca^{2+}-Binding Domain of Nucleobindin. The fragment of human nucleobindin studied by NMR encompasses residues 228−326 of the full-length protein. Here on, residues 228 and 326 will be designated residues 1 and 99, respectively.

The ^{15}N-HSQC spectrum of the Ca^{2+}-binding domain of nucleobindin loaded with Ca^{2+} shows amide protons with low-field-shifted chemical shifts (Figure 2A), which is a typical feature of EF-hand motifs (*31*−*33*). In the absence of Ca^{2+}, the ^{15}N-HSQC spectrum loses chemical shift dispersion and looks like the spectrum expected for an unstructured protein (Figure 2B). The difference between both spectra indicates that Ca^{2+} has a profound effect on the conformation of the protein.

Figure 1B shows the alignment of the amino acid sequences belonging to EF-hand loops of several proteins acting as Ca^{2+} buffers and Ca^{2+} sensors. The characteristic glycine is substituted by an arginine residue at position 310 (83 in the numeration used here) in nucleobindin.

The backbone and side chain chemical shift assignments indicate that the two amide protons that are low-field-shifted upon addition of Ca^{2+} belong to residues Gly31 and Arg83, which are located at the sixth position of the first and second 12-residue loops.

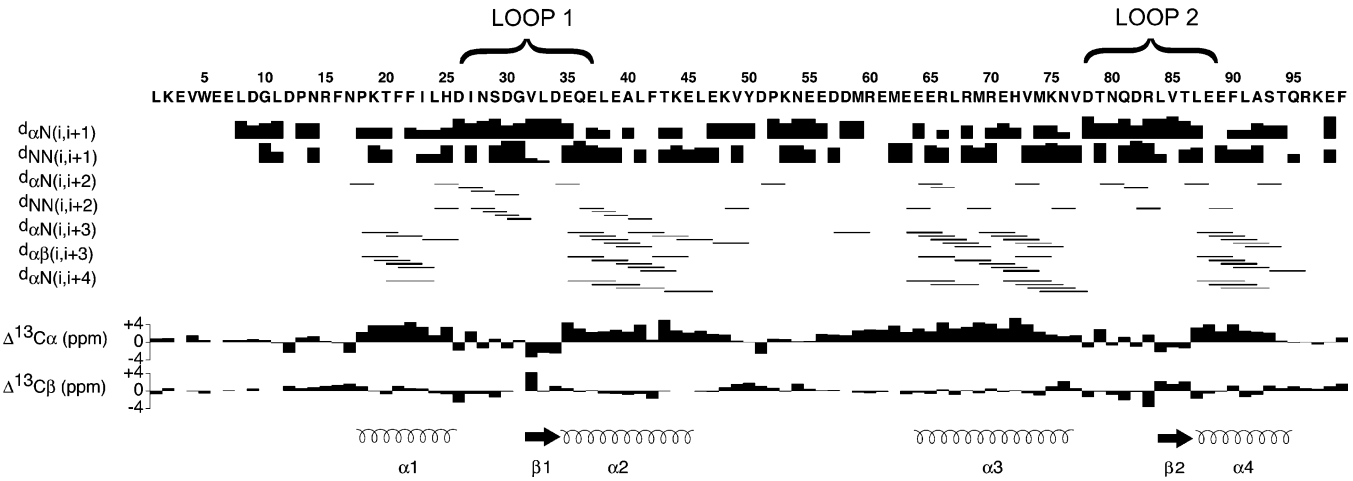

FIGURE 3: Schematic representation of the secondary structure of the Ca^{2+}-binding domain of human nucleobindin on the basis of short- and medium-range NOE contacts, as well as $^{13}C_\alpha$,$^{13}C_\beta$ secondary shifts. The location of the Ca^{2+}-binding loops is shown.

$^{13}C_\alpha$ and $^{13}C_\beta$ backbone secondary shifts (*34*) and short-range NOE analysis (*35*) show that the structure of nucleobindin is comprised of four α-helices and two β-strands (Figure 3). Secondary shifts agree with the presence of three N-cap residues at the beginning of helices I, II, and IV (Figure 3). These N-terminal helix-capping motifs have been observed previously in other Ca^{2+}-binding proteins such as calmodulin (*36*).

The three-dimensional solution structure of the Ca^{2+}-binding domain of nucleobindin was solved using distance restraints derived from NOE data and residual dipolar couplings obtained from the protein partial alignment by liquid crystals in the magnetic field. Table 1 summarizes the structural statistics calculated for the 20 lowest energy conformers. For all nonflexible regions, 85% of the residues have ϕ and ψ angles belonging to the most favored regions of the Ramachandran plot. The backbone RMSD obtained by superimposing all structures is 0.41 Å, which indicates that the structure calculation leads to a precise ensemble of NMR conformers. The three-dimensional arrangement of the four α-helices and the two β-strands is represented as a ribbon diagram in Figure 4A. The calculated structure is that of two consecutive EF-hand folds, a structure commonly adopted by many Ca^{2+}-binding proteins. The atomic coordinates of the structures, as well as the restraints used in the structure calculation, coordinates of the alignment tensor, and chemical shift assignment, are deposited in the Protein Data Bank with accession code 1SNL. Chemical shift assignment is also deposited in the BioMagResBank (BMRB) with accession number 6167.

As previously mentioned, the amino acid sequence of the C-terminal EF-hand in nucleobindin departs from the consensus EF-hand sequence (Figure 1B). This can lead to the assumption that the conformation of the EF-hand may be different and that this, in turn, may affect the Ca^{2+}-binding capability. Therefore, it is important to evaluate the ϕ and ψ angles adopted by all the residues involved in both EF-hand moieties. As shown in Figure 5, the average ϕ and ψ values calculated from the 20 lowest energy conformers are very similar for residues in equivalent positions of the two EF-hand moieties. The most representative pairs of equivalent residues with similar location in the Ramachandran map are Ser29/Gln81 and Gly31/Arg83, which adopt left-handed α-helical angles that are uncommon for all 20 amino acids except for glycine (*37*). It is worth noting that no angle restraints for these residues were used in the structure calculation.

Table 1: Structural Statistics for the Solution Structure of the Calcium-Binding Domain of Human Nucleobindin (Calnuc)[a]

restraints	RMSD: 20 lowest energy conformers	RMSD: lowest energy conformer
distances (Å) (1463)		
intraresidue (733)	0.042 ± 0.002	0.039
sequential $\|i-j\|=1$ (308)	0.032 ± 0.003	0.033
short-range $\|i-j\| \le 5$ (237)	0.028 ± 0.004	0.025
long-range $\|i-j\| \ge 5$ (185)	0.036 ± 0.002	0.032
hydrogen bonds (Å) (26)	0.021 ± 0.003	0.029
dihedrals (deg) (88)	0.8 ± 0.1	0.7
residual dipolar couplings (Hz) (223)		
$^1D_{NH}$ (Pf1) (73)	2.1 ± 0.1	2.0
$^1D_{C\alpha C'}$ (Pf1) (62)	0.89 ± 0.03	0.91
$^1D_{C\alpha H}$ (Pf1) (53)	0.90 ± 0.07	0.93
$^1D_{C\beta H\beta}$ (Pf1) (6)[b]		
$^1D_{CH3}$ (Pf1) (29)[b]		
deviations from idealized covalent geometry		
bonds (Å) (1663)	0.0045 ± 0.0001	0.0043
angles (deg) (3005)	0.58 ± 0.01	0.56
impropers (deg) (853)	0.41 ± 0.03	0.38
structure quality		
Lennard-Jones[c] potential energy (kcal mol^{-1})	−340 ± 18	−339
Ramachandran plot analysis[d]: residues 18−46, 64−94	85.1% ± 2%	84.5%
coordinate precision[e]		
residues 18−46, 64−94		
backbone (N, Cα, C′,O)	0.41 ± 0.07 Å	
all non-H atom	1.04 ± 0.06 Å	

[a] The statistics were performed using the 20 conformers with the lowest overall energies. These conformers have no NOE or dihedral angle restraint violations greater than 0.41 Å and 5°, respectively. [b] Residual dipolar couplings for side chains and backbone atoms of high flexibility are not included in the statistics. [c] The Lennard-Jones van der Waals energy was calculated with the CHARMM PARAM19/20 parameters and was not included in structure calculation. [d] Procheck (*58*) analysis gives 0.0% of the residues in a disallowed regions of the Ramachandran map for the nonflexible regions. The percentage given accounts for residues in the most favored regions of the Ramachandran map. [e] The RMSD is reported between the 20 conformers and the mean coordinates.

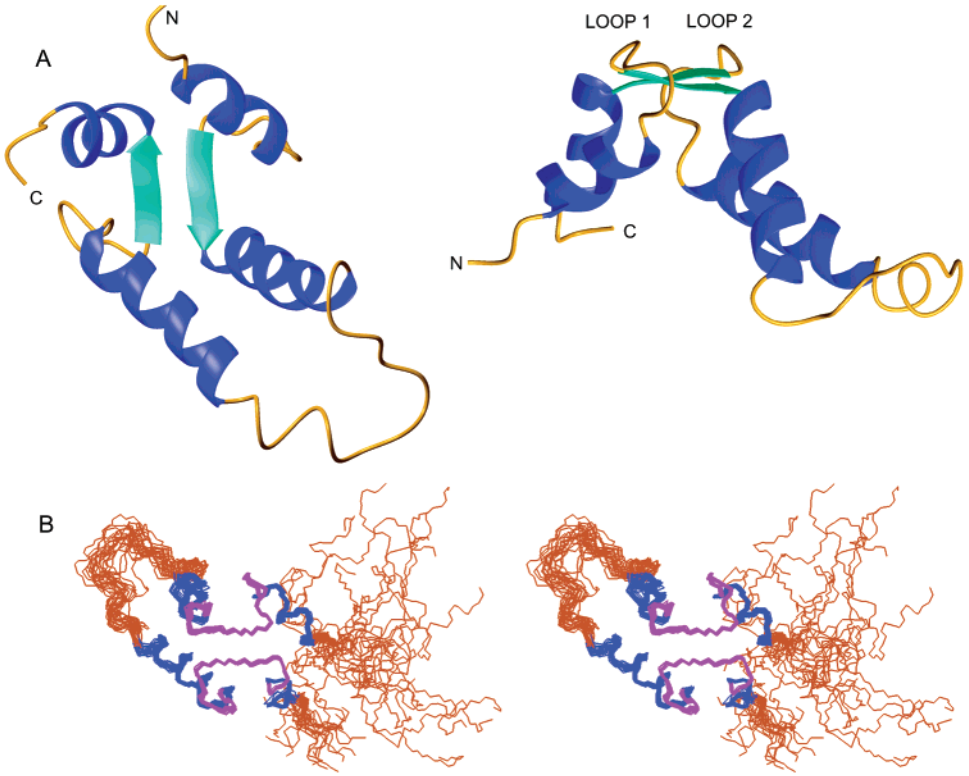

FIGURE 4: (A) Ribbon diagrams of the tertiary fold of human nucleobindin's EF-hand motifs with the location of the Ca^{2+}-binding loops indicated; (B) stereoview superposition of the 20 lowest energy conformers of the Ca^{2+}-binding domain of human nucleobindin. The β-sheet is on top. The 12-residue Ca^{2+}-binding loops are colored in magenta. The rest of the helices are colored in blue. Orange regions indicate conformational heterogeneity. The long and short flexible tails are the N- and C-terminus, respectively. Figure 4 was created using the program MOLMOL (*59*).

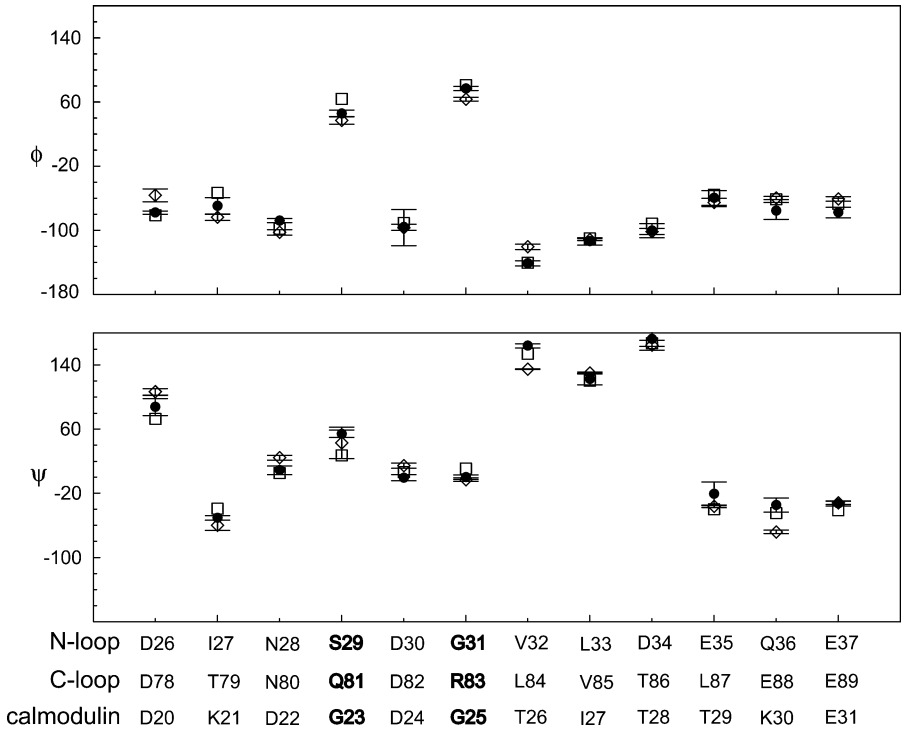

FIGURE 5: Averaged ϕ and ψ angles over the 20 lowest energy conformers of each residue in the 12-residue Ca^{2+}-binding loop of nucleobindin. Filled circles and open diamonds correspond to the N- and C-terminal EF-hand, respectively. The ϕ and ψ angles of the N-terminal EF-hand of the 1 Å crystal structure of calmodulin (open squares) (*60*) are shown as an example of a canonical EF-hand. Residues in the left-handed α-helical region of the Ramchandran map are highlighted in bold.

The superposition of the 20 lowest energy conformers is shown in Figure 4B. The regions of the protein in which the structures show large conformational variability coincide with the regions of high mobility according to the ^{15}N NMR relaxation analysis (vide infra). The β-sheet, α-helices, and Ca^{2+}-binding loops are rigid. In contrast, the helix termini

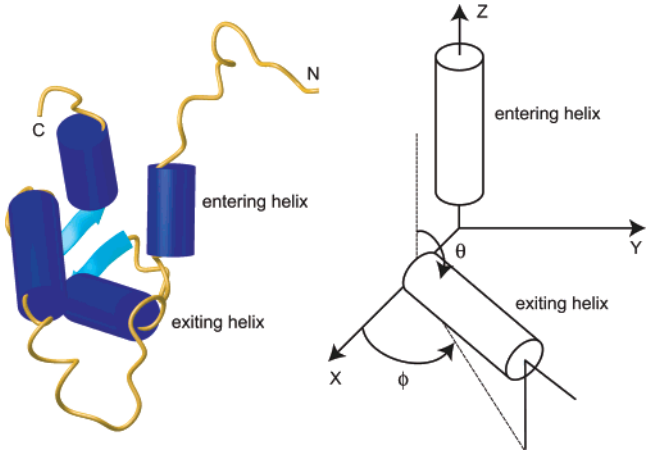

FIGURE 6: Cylindrical representation of the two EF-hand motifs of human nucleobindin (left) and cylinders and axis system of reference and angle definition (right). The N-terminal EF-hand of nucleobindin has been oriented to match the axis and cylinders of reference. The left-hand side of Figure 6 was created using the program MOLMOL (*59*).

that are connected by the linker between both EF-hand motifs are not as well structured.

Comparison with Other EF-Hand Structures. Members of the EF-hand superfamily show a large variability of conformations depending on the relative orientation of the helices. Three major conformations have been classified, the open, the closed, and the semiopen conformation (*38*). Ca^{2+}-free EF-hand motifs usually fold into the closed conformation. A large rearrangement of the helices induced by Ca^{2+} binding leads to the open conformation, which in turn results in the exposure of large hydrophobic surfaces that are usually targets for protein−protein interactions. The semiopen conformation has only been found in the essential and regulatory light chains of myosin (*39*). This classification is based on the interhelical angles obtained from crystal and NMR structures of EF-hand proteins in the apo- and holo-states.

The Ca^{2+}-induced conformational change is common in EF-hand proteins that act as Ca^{2+} sensors. Ca^{2+}-binding leads to protein−protein interactions that activate or inhibit the function of the target (*40*). In contrast, EF-hand proteins that function as Ca^{2+} buffers undergo only minor structural changes upon Ca^{2+} binding. Calbindin D_{9k} has been reported as an example of this behavior (*38*).

According to our NMR data, nucleobindin is unstructured in the absence of Ca^{2+}, and it folds into two EF-hand motifs upon Ca^{2+} addition. This result indicates that Ca^{2+} has a profound stabilizing effect in the Ca^{2+}-binding domain of nucleobindin.

The EF-hand structure can be quantitatively characterized by the values of the interhelical angles in the helix-loop-helix motif. The vector geometry mapping method has been reported recently as an efficient method to characterize and classify EF-hand proteins and to study the conformational changes associated with Ca^{2+}-binding (*41*). This method uses a cylindrical representation of the helices to measure the angle θ between the entering N-terminal and exiting C-terminal helices of the EF-hand, as well as the angle ϕ between the *X* axis of reference and the projection of the exiting helix in the XY plane (Figure 6). With the use of this method, the N-terminal EF-hand of nucleobindin has angles $\theta = 87.8°$, $\phi = 85.2°$ and the C-terminal EF-hand has angles $\theta = 78.4°$, $\phi = -152.8°$. According to a previously reported study on 90 EF-hand motifs using the first EF-hand moiety of apo-calmodulin as reference axis, 89% have θ angles in the range $30° < \theta < 90°$ and 80% have ϕ angles in the range $80° < \phi < 140°$ (*38*). The θ and ϕ angles of the canonical (N-terminal) EF-hand motif of nucleobindin fall within the average values found for other EF-hand structures. The ϕ value for the noncanonical (C-terminal) EF-hand deviates from the average range.

θ angles close to 90° correspond to the open conformation (*38*), which is the one adopted in Ca^{2+}-bound EF-hand motifs. Both EF-hand folds in nucleobindin adopt the open conformation.

In Ca^{2+} sensor proteins, the open conformation is associated with the exposure of hydrophobic surface. Figure 7 shows the structures of Ca^{2+}-bound calbindin D_{9k} (*42*), nucleobindin, C-terminal domain of calmodulin (*43*), and the Ca^{2+}-free C-terminal domain of calmodulin (*44*), highlighting solvent-exposed hydrophobic area. All four are NMR structures. For a better comparison regarding the number of EF-hand motifs present, the structure of the C-terminal domain of calmodulin is shown. The total solvent-accessible area for the different structures is as follows: 4748 Å^2 for calbindin D_{9k}, 4990 and 5799 Å^2 for the Ca^{2+}-free and Ca^{2+}-bound C-terminal domain of calmodulin, respectively, and 7141 Å^2 for nucleobindin. The increase in solvent-exposed surface area of the C-terminal domain of calmodulin is associated with the opening of the structure upon Ca^{2+}-binding. The EF-hand domain of nucleobindin is more open than the other three structures. The four proteins or domains have a similar number of amino acids. The solvent-exposed hydrophobic surface area out of the total accessible surface is 19% for calbindin D_{9k}, 23% for the Ca^{2+}-bound C-terminal domain of calmodulin, and 26% for nucleobindin. These percentages were calculated considering the apolar residues alanine, valine, isoleucine, leucine, methionine, phenylalanine, tyrosine, tryptophan, and histidine. The increase in solvent-accessible surface of calmodulin (∼800 Å^2) upon Ca^{2+} binding agrees with its ability to interact with peptides.

Ca^{2+}-Binding Capability of Nucleobindin. Nucleobindin undergoes a structural change upon Ca^{2+}-binding that can be monitored by NMR. In the absence of Ca^{2+}, nucleobindin lacks a well-structured three-dimensional fold as revealed by the small amide ^{1}H chemical shift dispersion (7.6−8.5 ppm) of the ^{15}N-HSQC spectrum (Figure 2B). Upon Ca^{2+} addition, new NMR signals appear, which coexist with the signals of the apo-form, indicating that the conformational change has a slow rate in the NMR time scale (Figure 8A). The intensity of these signals increases with the concentration of Ca^{2+}, and the signals belonging to the Ca^{2+}-free form decrease in intensity until only one set of signals, which corresponds to the Ca^2-bound form, is observed. NMR signals characteristic of both EF-hand moieties appear almost simultaneously upon Ca^{2+} addition. Furthermore, the structural change induced by Ca^{2+}-binding affects the whole domain and not only the residues involved in Ca^{2+}-binding. These results suggest that Ca^{2+} affinities are similar in both loops, and Ca^{2+}-binding does not occur sequentially for each EF-hand.

We monitored signal intensity increase upon Ca^{2+} binding for four low-field-shifted amide ^{1}H signals of two residues

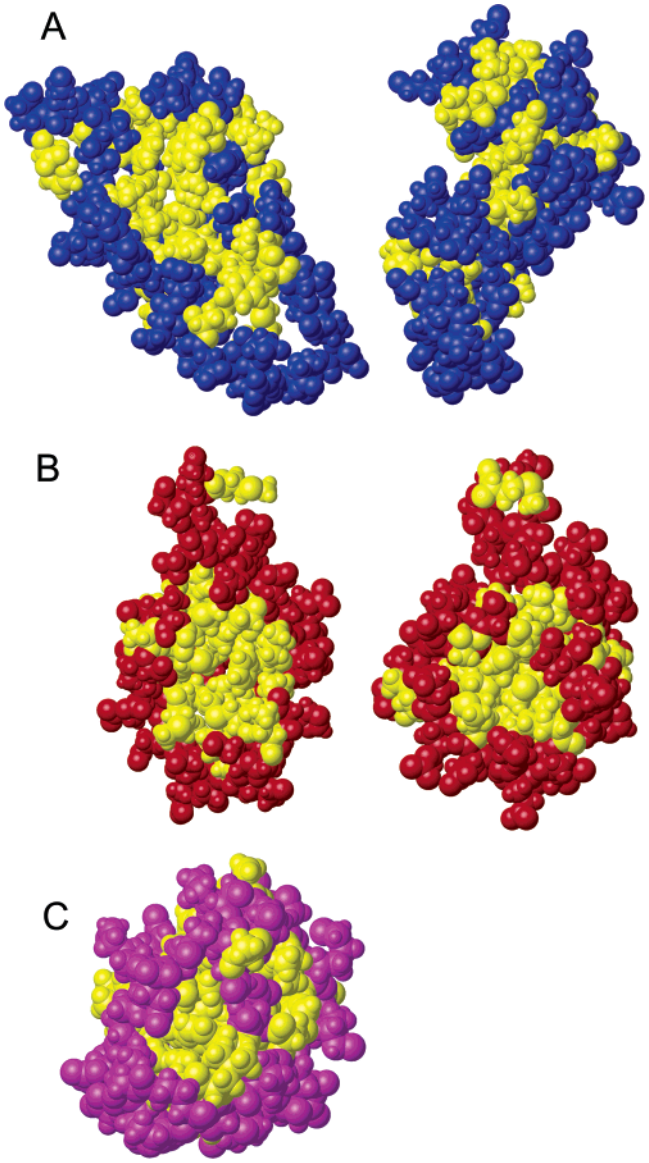

FIGURE 7: (A) Atom-filled representation of nucleobindin (left, front view; right, side view); (B) Ca^{2+}-loaded C-terminal domain of calmodulin (left) and Ca^{2+}-free C-terminal domain of calmodulin (right); (C) Ca^{2+}-loaded calbindin D_{9K}. Atoms of apolar residues are colored in yellow (i.e., alanine, valine, isoleucine, leucine, methionine, phenylalanine, tyrosine, histidine, tryptophan). The orientation of all proteins (front view of nucleobindin) is equivalent, matches that represented in Figure 4A, and shows the hydrophobic area that should be exposed upon target binding. Figure 7 was generated using the program MOLMOL (*59*).

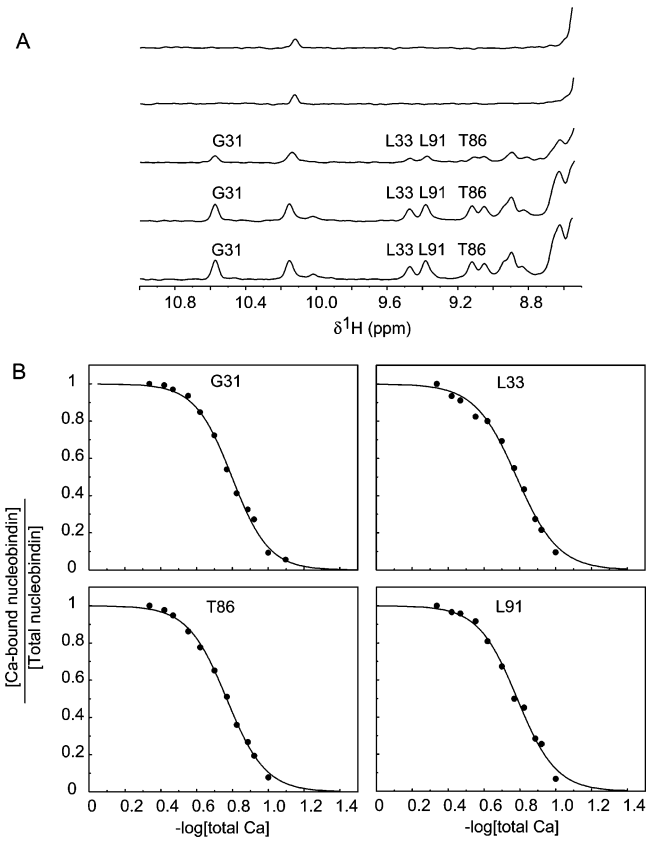

FIGURE 8: (A) One-dimensional projection of ^{15}N-HSQC spectra of the EF-hand domain of human nucleobindin at different Ca^{2+} concentrations (from top to bottom, 0, 0.08, 0.13, 0.24, and 0.34 mM $CaCl_2$). Residues of which the signal intensity was measured throughout the titration are indicated. (B) Fitting of signal intensity change upon Ca^{2+}-addition to the equation; $y = (A_0 + A_1 \times 10^{A_3(x-A_2)})/(1 + 10^{A_3(x-A_2)})$. Calculated values of the apparent K_d are G31 (39.9 μM), L33 (40 μM), T86 (51.1 μM), and L91 (43.0 μM).

belonging to each helix-loop-helix motif (Figure 8A). In principle, two different equilibria are present, that is, the equilibrium associated with Ca^{2+} binding and that of the structural change. An apparent Ca^{2+}-dissociation constant (K_d) has been measured for each EF-hand (Figure 8B). Since Ca^{2+} affinity constants of EF-hand motifs are usually measured neglecting the presence of Ca^{2+}-derived conformational changes, the K_d values reported herein can be compared to previously reported EF-hand Ca^{2+}-dissociation constants. Assuming a single equilibrium constant for the overall structural change, the measured K_d values indicate that both EF-hand structures have similar Ca^{2+} affinity.

It is not possible to get direct evidence of the presence of Ca^{2+} in each helix-loop-helix motif by NMR, because Ca^{2+} is magnetically inactive. In principle, it could be argued that the low-field-shifted NMR signals of one EF-hand are a consequence of the structural perturbation caused by Ca^{2+}-binding in the other EF-hand. However, 2 equiv of Ca^{2+} per equivalent of protein are necessary to finish the titration, which indicates that both EF-hands are able to bind Ca^{2+}, despite the noncanonical sequence of the C-terminal EF-hand.

Attempts were made to substitute Ca^{2+} for the lanthanides Yb^{3+} and Tb^{3+}, to obtain direct evidence of metal binding in both EF-hands, and to gain structural information about metal position through pseudocontact shifts (*45*). Even in the presence of high salt concentrations (400 mM KCl or 400 mM NaCl), which decrease protein−lanthanide nonspecific binding (*46*), only NMR signals of residues that are close to Ca^{2+} were unmodified upon lanthanide addition, while a large number of other NMR signals broadened and disappeared (data not shown). This result indicates that the lanthanides bind nonspecifically to the protein surface and are not able to replace Ca^{2+}.

^{15}N NMR Relaxation Studies on the Ca^{2+} Binding Domain of Nucleobindin. NMR signals of the ^{15}N-HSQC spectrum of nucleobindin are slightly broader than expected for its molecular weight (Figure 2A). In addition, the number of long-range NOEs is in the low range for a molecule of 99 amino acids (Table 1). To gain information on the dynamic

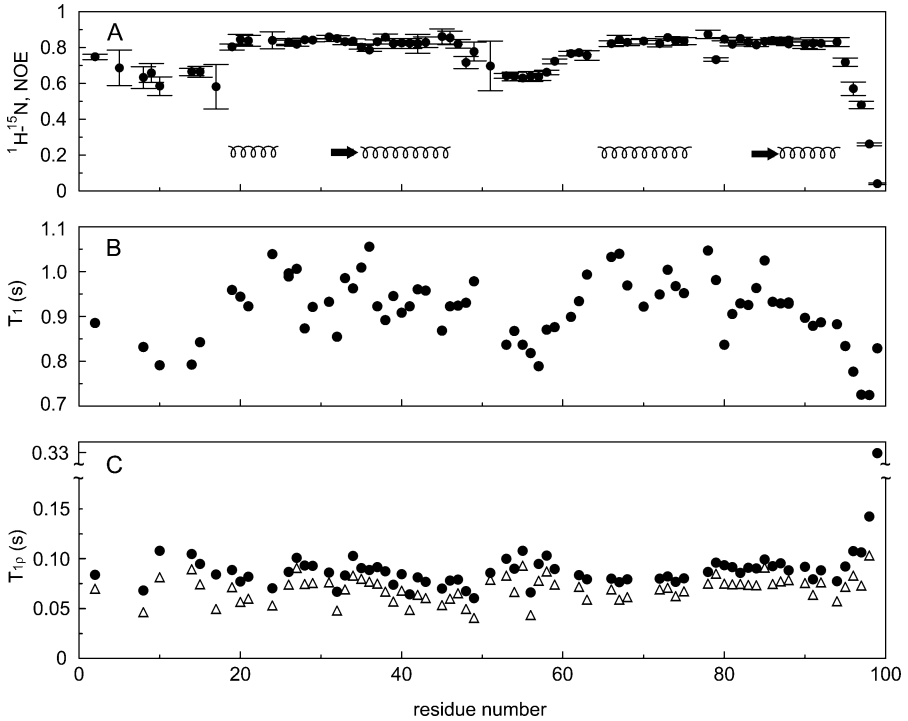

FIGURE 9: ^{15}N spin relaxation data on the Ca^{2+}-binding domain of human nucleobindin. Panel A shows $^1H-^{15}N$ heteronuclear NOE at 800 MHz. Errors represented by thin bars are based on signal-to-noise ratio. Panel B shows T_1 at 800 MHz. Panel C shows $T_{1\rho}$ at 800 MHz (△) and 600 MHz (●). The error is 0.04%, 4.1%, and 3.1% of the measurement based on signal-to-noise ratio for T_1, $T_{1\rho}$ at 800 MHz, and $T_{1\rho}$ at 600 MHz, respectively. The secondary structural elements are indicated in panel A.

behavior of the EF-hand domain of nucleobindin, ^{15}N spin relaxation experiments were performed at two magnetic fields, 600 and 800 MHz, and different protein concentrations. Longitudinal (T_1) and transverse ($T_{1\rho}$) ^{15}N spin relaxation times, together with $^1H-^{15}N$ heteronuclear NOE, were obtained for ~70 residues (Figure 9). Overlapping amide NMR signals are not included, and some were not observed due to chemical exchange with water.

According to $^1H-^{15}N$ NOE data, there are three regions in the Ca^{2+}-binding domain of nucleobindin with high flexibility characteristic of disordered conformations (Figure 9A). These are the N-terminus up to residue P18 (starting residue of the first α-helix), the 18-residue linker between both EF-hand motifs, and the five C-terminal residues. Flexibility agrees with the absence of short-, medium-, or long-range $^1H-^1H$ NOE contacts of residues located in these regions. The α-helices and β-strands, as well as the Ca^{2+}-binding loops, have heteronuclear NOE values characteristic of secondary structural elements (~0.85). Only the first two residues of helix II (E35 and Q36) and residue T79 in the C-terminal loop possess low values of the heteronuclear NOE, indicative of a higher degree of flexibility (Figure 9A). Our data agree with previously reported NMR dynamic studies on the holo-forms of calmodulin (*47*), calbindin D_{9k} (*48*), and the calcium vector protein (*49*) in that high flexibility is observed in the linker between the EF-hand motifs, while the α-helices and the Ca^{2+}-binding loops are well ordered. Calcium-loaded parvalbumin is an exception, since it has been shown to be more rigid than calbindin D_{9k} or calmodulin, even in the linker region (*50*). In contrast, the absence of Ca^{2+} seems to introduce flexibility in the Ca^{2+}-binding loops, as shown for the apo-forms of troponin C (*51*), S100B (*52*), and calbindin D_{9k} (*53*).

Transverse ^{15}N relaxation times of nucleobindin at both magnetic fields and two protein concentrations (0.9 and 0.02 mM) are unusually scattered along the amino acid sequence (Figure 9C). This result indicates the presence of slow motion, conformational exchange, or both. The scatter decreases when approaching the C-terminal EF-hand and is small from residue N80 to F90. The average $T_{1\rho}$ value at 0.9 mM protein concentration is 85.5 ± 12.5 ms at 600 MHz and 69.6 ± 11.3 ms at 800 MHz, excluding the N- and C-termini. The error in the measurement is 3.7 ms, approximately 3 times smaller than the observed scatter.

A similar average transverse relaxation time (85.5 ± 16.0 ms) at 600 MHz and 0.02 mM protein concentration indicates that protein self-association can be ruled out as a possible factor affecting ^{15}N relaxation data.

NMR relaxation results together with the presence of broad NMR signals, as well as a large solvent-exposed protein surface, suggest that the EF-hand motifs of nucleobindin are not as compact as a typical globular domain, which could be a result of high flexibility or conformational exchange.

The Ca^{2+}-binding domain of nucleobindin folds independently of the rest of the protein into two EF-hand motifs. However, it cannot be ruled out that other domains in the full-length protein may have an effect in its dynamic behavior. In the absence of the rest of the protein, the Ca^{2+}-binding domain might be less stable. This could be a possible reason of why the Ca^{2+}-binding domain of nucleobindin is less compact.

CONCLUSIONS

Nucleobindin has been shown to function as a Ca^{2+} storage protein in the Golgi. Additionally, it is able to interact with other proteins through its EF-hand domain. Therefore,

biochemical data suggest that nucleobindin may act as Ca^{2+} buffer and as Ca^{2+} sensor.

Ca^{2+}-binding produces a conformational change in EF-hand proteins that function as Ca^{2+} sensors. This structural change is associated with the exposure of a hydrophobic surface, otherwise hidden in the Ca^{2+}-free protein. In contrast, proteins acting as Ca^{2+} buffers undergo only small structural changes upon Ca^{2+}-binding.

The Ca^{2+}-induced structural change in nucleobindin points in favor of its function as a Ca^{2+} sensor. Its three-dimensional structure is open and exposes a large hydrophobic surface, like Ca^{2+}-bound calmodulin, suggesting its potential ability to interact with other proteins.

The measured Ca^{2+} dissociation constants are closer to values reported for Ca^{2+} sensors and indicate a lower Ca^{2+} affinity than what is expected for a Ca^{2+} buffer. Ca^{2+} dissociation constants that do not fall within the range of Ca^{2+} sensors or Ca^{2+} buffers have been attributed to proteins that may perform both functions, such as calbindin D_{28k} (*54*).

It is unusual in the EF-hand protein superfamily to lack tertiary structure in the absence of Ca^{2+}. Troponin C, calmodulin, and calbindin D_{9k} have well-defined tertiary folds in the apo-form. The calcium vector protein is an exception, since it does not have tertiary structure in the apo-state (*55*). The physiological relevance of an unfolded protein under native conditions is not known, but it has been related to a need of higher flexibility that facilitates molecular recognition (*56*, *57*).

Our structural data on the Ca^{2+}-binding domain of nucleobindin, and the measured calcium-dissociation constants agree with its function as a calcium sensor. However, nucleobindin has been shown to function as a calcium storage protein too. It is possible that the unusually large solvent-accessible surface indicative of a very open conformation and its unfolded state in the calcium-free form, together with the high degree of dynamic or conformational flexibility, are particular features of nucleobindin that facilitate its dual function as a Ca^{2+} buffer and a Ca^{2+} sensor depending on the needs of the cell.

ACKNOWLEDGMENT

We are grateful to Drs. Marylin Gist Farquhar and Ping Lin for providing nucleobindin (calnuc) c-DNA. We thank Dr. Hank Fales for acquiring mass spectra on the Ca^{2+}-binding domain of nucleobindin and Dr. Victor Munoz for reading the manuscript and useful suggestions.

REFERENCES

1. Nelson, M. R., Thulin, E., Fagan, P. A., Forsen, S., and Chazin, W. J. (2002) The EF-hand domain: A globally cooperative structural unit, *Protein Sci. 11*, 198−205.
2. Miura, K., Titani, K., Kurosawa, Y., and Kanai, Y. (1992) Molecular cloning of nucleobindin, a novel DNA-binding protein that contains both a signal peptide and a leucine zipper structure, *Biochem. Biophys. Res. Commun. 187*, 375−380.
3. Lin, P., Le-Niculescu, H., Hofmeister, R., McCaffery, J. M., Jin, M., Hennemann, H., McQuistan, T., De Vries, L., and Farquhar, M. G. (1998) The mammalian calcium-binding protein, nucleobindin (CALNUC), is a Golgi resident protein, *J. Cell Biol. 141*, 1515−1527.
4. Lin, P., Yao, Y., Hofmeister, R., Tsien, R. Y., and Farquhar, M. G. (1999) Overexpression of CALNUC (Nucleobindin) increases agonist and thapsigargin releasable Ca^{2+} storage in the Golgi, *J. Cell Biol. 145*, 279−289.
5. Weiss, T. S., Chamberlain, C. E., Takeda, T., Lin, P., Hahn, K. M., and Farquhar, M. G. (2001) Gαi3 binding to calnuc on Golgi membranes in living cells monitored by fluorescence resonance energy transfer of green fluorescent protein fusion proteins, *Proc. Natl. Acad. Sci. U.S.A. 98*, 14961−14966.
6. Lin, P., Fischer, T., Weiss, T. S., and Farquhar, M. G. (2000) Calnuc, an EF-hand Ca^{2+} binding protein, specifically interacts with the C-terminal α5-helix of Gαi3, *Proc. Natl. Acad. Sci. U.S.A. 97*, 674−679.
7. Lavoie, C., Meerloo, T., Lin, P., and Farquhar, M. G. (2002) Calnuc, an EF-hand Ca^{2+}-binding protein, is stored and processed in the Golgi and secreted by the constitutive-like pathway in AtT20 cells, *Mol. Endocrinol. 16*, 2462−2474.
8. Mochizuki, N., Hibi, M., Kanai, Y., and Insel, P. A. (1995) Interaction of the protein nucleobindin with Gαi2, as revealed by the yeast two-hybrid system, *FEBS Lett. 373*, 155−158.
9. Miura, K., Kurosawa, Y., and Kanai, Y. (1994) Calcium-binding activity of nucleobindin mediated by an EF hand moiety, *Biochem. Biophys. Res. Commun. 199*, 1388−1393.
10. Wendel, M., Sommarin, Y., Bergman, T., and Heinegard, D. (1995) Isolation, characterization, and primary structure of a calcium-binding 63-kDa bone protein, *J. Biol. Chem. 270*, 6125−6133.
11. Kanai, Y., Takeda, T., Miura, K., Amagai, M., Kanedo, T., Kubota, T., Kanai, Y., Tanuma, S.-I., and Kurosawa, Y. (1995) Induction of autoantibodies in normal mice by injection of nucleobindin and natural occurrence of antibodies against nucleobindin in autoimmune MRL/*lpr*/*lpr* mice, *Immunol. Lett. 45*, 35−42.
12. Kanai, Y., Kyuwa, S., Miura, K., and Kurosawa, Y. (1995) Induction and natural occurrence of serum nucleosomal DNA in autoimmune MRL/*lpr*/*lpr* mice: its relation to apoptosis in the thymus, *Immunol. Lett. 46*, 207−214.
13. Ballif, B. A., Mincek, N. V., Barratt, J. T., Wilson, M. L., and Simmons, D. L. (1996) Interaction of cyclooxygenases with apoptosis- and autoimmunity-associated protein, *Proc. Natl. Acad. Sci. U.S.A. 93*, 5544−5549.
14. Taniguchi, N., Taniura, H., Niinobe, M., Takayama, C., Tominaga-Yoshino, K., Ogura, A., and Yoshikawa, K. (2000) The postmitotic growth suppressor necdin interacts with a calcium-binding protein (NEFA) in neuronal cytoplasm, *J. Biol. Chem. 275*, 31674−31681.
15. Slupsky, C. M., and Sykes, B. D. (1999) in *Calcium as a cellular regulator* (Klee, E. C. a. C., Ed.) pp 73−99, Oxford University Press, New York.
16. Bax, A., and Grzesiek, S. (1993) Methodological advances in protein NMR, *Acc. Chem. Res. 26*, 131−138.
17. Ottiger, M., Delaglio, F., Marquardt, J. L., Tjandra, N., and Bax, A. (1998) Measurement of dipolar couplings from methylene and methyl sites in weakly oriented macromolecules and their use in structure determination, *J. Magn. Reson. 134*, 365−369.
18. Delaglio, F., Grzesiek, S., Vuister, G. W., Zhu, G., Pfeifer, J., and Bax, A. (1995) NMRPipe: A multidimensional spectral processing system based on UNIX Pipes, *J. Biomol. NMR 6*, 277−293.
19. Garrett, D. S., Powers, R., Gronenborn, A. M., and Clore, G. M. (1991) A common sense approach to peak picking in two-, three- and four dimensional spectra using automatic computer analysis of contour diagrams, *J. Magn. Reson. 95*, 214−220.
20. Marion, D., Ikura, M., Tschudin, R., and Bax, A. (1989) Rapid recording of 2D NMR spectra without phase cycling. Application to the study of hydrogen exchange in proteins, *J. Magn. Reson. 85*, 393−399.
21. Barbato, G., Ikura, M., Kay, L. E., Pastor, R. W., and Bax, A. (1992) Backbone dynamics of calmodulin studied by ^{15}N relaxation using inverse detected two-dimensional NMR spectroscopy: the central helix is flexible, *Biochemistry 31*, 5269−5278.
22. Piotto, M., Saudek, V., and Sklenar, V. (1992) Gradient-tailored excitation for single-quantum NMR spectroscopy of aqueous solutions, *J. Biomol. NMR 2*, 661−665.
23. Bax, A., and Pochapsky, S. S. (1992) Optimized recording of heteronuclear multidimensional NMR spectra using pulse field gradients, *J. Magn. Reson. 99*, 638−643.
24. Grzesiek, S., and Bax, A. (1993) Amino acid type determination in the sequential assignment procedure of uniformly $^{13}C/^{15}N$ enriched proteins, *J. Biomol. NMR 3*, 185−204.
25. Peng, J. W., Thanabal, V., and Wagner, G. (1991) Improved accuracy of heteronuclear transverse relaxation time measurements in macromolecules. Elimination of antiphase contributions, *J. Magn. Reson. 95*, 421−427.

26. Grzesiek, S., and Bax, A. (1993) The importance of not saturating water in protein NMR. Application to sensitivity enhancement and NOE measurements, *J. Am. Chem. Soc. 115*, 12593−12594.
27. Brunger, A. T. (1993) *X-PLOR Version 3.1: A system for X-ray crystallography and NMR*, Yale University Press, New Haven, Connecticut.
28. Tjandra, N., Omichinski, J. G., Gronenborn, A., Clore, M. G., and Bax, A. (1997) Use of dipolar ^{1}H-^{15}N and ^{1}H-^{13}C couplings in the structure determination of magnetically oriented macromolecules in solution, *Nat. Struct. Biol. 4*, 732−738.
29. Clore, M. G., Gronenborn, A. M., and Bax, A. (1998) A robust method for determining the magnitude of the fully asymmetric alignment tensor of oriented macromolecules in the absence of structural information, *J. Magn. Reson. 133*, 216−221.
30. Cornilescu, G., Delaglio, F., and Bax, A. (1999) Protein backbone angle restraints from searching a database for chemical shift and sequence homology, *J. Biomol. NMR 13*, 289−302.
31. Kordel, J., Skelton, N. J., Akke, M., and Chazin, W. J. (1993) High-resolution solution structure of calcium-loaded calbindin D_{9k}, *J. Mol. Biol. 231*, 711−734.
32. Spyracopoulos, L., Li, M. X., Sia, S. K., Gagne, S. M., Chandra, M., Solaro, R. J., and Sykes, B. D. (1997) Calcium-induced structural transition in the regulatory domain of human cardiac troponin C, *Biochemistry 36*, 12138−12146.
33. Zhang, M., Tanaka, T., and Ikura, M. (1995) Calcium-induced conformational transition revealed by the solution structure of apo calmodulin, *Nat. Struct. Biol. 2*, 758−767.
34. Wishart, D. S., Sykes, B. D., and Richards, F. M. (1991) Relationship between Nuclear Magnetic Resonance Chemical Shift and Protein Secondary Structure, *J. Mol. Biol. 222*, 311−333.
35. Wuthrich, K. (1986) *NMR of proteins and nucleic acids*, John Wiley & Sons, New York.
36. Gronenborn, A. M., and Clore, M. G. (1994) Identification of N-terminal helix capping boxes by means of ^{13}C chemical shifts, *J. Biomol. NMR 4*, 455−458.
37. Wilmot, C. M., and Thornton, J. M. (1988) Analysis and prediction of the different types of beta-turn in proteins, *J. Mol. Biol. 203*, 221−232.
38. Yap, K. L., Ames, J. B., Swindells, M. B., and Ikura, M. (1999) Diversity of conformational states and changes within the EF-hand protein superfamily, *Proteins 37*, 499−507.
39. Houdusse, A., and Cohen, C. (1995) Target sequence recognition by the calmodulin superfamily: implications from the light chain binding to the regulatory domain of scallop myosin, *Proc. Natl. Acad. Sci. U.S.A. 92*, 10644−10647.
40. Crivici, A., and Ikura, M. (1995) Molecualr and structural basis of target recognition by calmodulin, *Annu. Rev. Biophys. Biomol. Struct. 24*, 85−116.
41. Yap, K. L., Ames, J. B., Swindells, M. B., and Ikura, M. (2002) Vector geometry mapping. A method to characterize the conformation of helix-loop-helix calcium-binding proteins, *Methods Mol. Biol. 173*, 317−324.
42. Akke, M., Drakenberg, T., and Chazin, W. J. (1992) Three-dimensional solution structure of the Ca^{2+}-loaded porcin calbindin D_{9k} determined by nucleoar magnetic resonance spectroscopy, *Biochemistry 31*, 1011−1020.
43. Finn, B. E., Evenas, J., Drakenberg, T., Waltho, J. P., Thulin, E., and Forsen, S. (1995) Calcium-induced structural changes and domain autonomy in calmodulin, *Nat. Struct. Biol. 2*, 777−783.
44. Finn, B. E., Drakenberg, T., and Forsen, S. (1993) The structure of apo-calmodulin: A ^{1}H NMR examination of the carboxy-terminal domain, *FEBS Lett. 336*, 368−374.
45. Lee, L., and Sykes, B. D. (1980) Strategies for the use of lanthanide NMR shift probes in the determination of protein structure in solution. Application to the EF calcium binding site of carp parvalbumin, *Biophys. J. 32*, 193−210.
46. Bertini, I., Gelis, I., Katsaros, N., Luchinat, C., and Provenzani, A. (2003) Tuning the affinity for lanthanides of calcium binding proteins, *Biochemistry 42*, 8011−8021.
47. Malmendal, A., Evenas, J., Forsen, S., and Akke, M. (1999) Structural dynamics in the C-terminal domain of calmodulin at low calcium levels, *J. Mol. Biol. 293*, 883−899.
48. Bertini, I., Carrano, C. J., Luchinat, C., Piccioli, M., and Poggi, L. (2002) A ^{15}N NMR mobility study on the dicalcium P43M calbindin D_{9k} and its mono-La^{3+}-substituted form, *Biochemistry 41*, 5104−5111.
49. Theret, I., Cox, J. A., Mispelter, J., and Craescu, C. T. (2001) Backbone dynamics of the regulatory domain of calcium vector protein, studied by ^{15}N relaxation at four fields, reveals unique mobility characteristics of the intermotif linker, *Protein Sci. 10*, 1393−1402.
50. Baldellon, C., Alattia, J.-R., Strub, M.-P., Pauls, T., Berchtold, M. W., Cave, A., and Padilla, A. (1998) ^{15}N NMR relaxation studies of the calcium-loaded parvalbumin show tight dynamics compared to those of other EF-hand proteins, *Biochemistry 37*, 9964−9975.
51. Spyracopoulos, L., Lavigne, P., Crump, M. P., Gagne, S. M., Kay, C. M., and Sykes, B. D. (2001) Temperature dependence of dynamics and thermodynamics of the regulatory domain of human cardiac troponin C, *Biochemistry 40*, 12541−12551.
52. Inman, K., Baldisseri, D. M., Miller, K. E., and Weber, D. J. (2001) Backbone dynamics of the calcium-signaling protein apo-S100B as determined by ^{15}N NMR relaxation, *Biochemistry 40*, 3439−3448.
53. Malmendal, A., Carlstrom, G., Hambraeus, C., Drakenberg, T., Forsen, S., and Akke, M. (1998) Sequence and context dependence of the EF-hand loop dynamics. An ^{15}N relaxation study of a calcium-binding site mutant of calbindin D_{9k}, *Biochemistry 37*, 2586−2595.
54. Berggard, T., Miron, S., Onnerfjord, P., Thulin, E., Akerfeldt, K. S., Enghild, J. J., Akke, M., and Linse, S. (2002) Calbindin D_{28k} exhibits properties characteristic of a Ca^{2+} sensor, *J. Biol. Chem. 277*, 16662−16672.
55. Theret, I., Baladi, S., Cox, J. A., Sakamoto, H., and Craescu, C. T. (2000) Sequential calcium binding to the regulatory domain of calcium vector protein reveals functional asymmetry and a novel mode of structural rearrangement, *Biochemistry 39*, 7920−7926.
56. Weinreb, P. H., Zhen, W., Poon, A. W., Conway, K. A., and Lansbury, P. T. J. (1996) NACP, a protein implicated in Alzheimer's disease and learning, is natively unfolded, *Biochemistry 35*, 13709−13715.
57. Lydakis-Simantiris, N., Hutchison, R. S., Betts, S. D., Barry, B. A., and Yocum, C. F. (1999) Manganese stabilizing protein of photosystem II is a thermostable, natively unfolded polypetide, *Biochemistry 38*, 404−414.
58. Laskowski, R. A., Rullman, J. A. C., MacArthur, M. W., Kaptein, R., and Thornton, J. M. (1996) AQUA and PROCHECK−NMR: Programs for checking the quality of protein structures solved by NMR, *J. Biomol. NMR 8*, 477−486.
59. Koradi, R., Billeter, M., and Wuthrich, K. (1996) MOLMOL: A program for display and analysis of macromolecular structures, *J. Mol. Graphics 14*, 51−55.
60. Wilson, M. A., and Brunger, A. T. (2000) The 1.0 Å crystal structure of Ca^{2+}-bound calmodulin: an analysis of disorder and implications for functionally relevant plasticity, *J. Mol. Biol. 301*, 1237−1256.

BI049310A